RESEARCH ARTICLE

Dual Roles of RNF2 in Melanoma Progression

Kunal Rai[1], Kadir C. Akdemir[1], Lawrence N. Kwong[1], Petko Fiziev[2,3,4], Chang-Jiun Wu[1], Emily Z. Keung[5,6], Sneha Sharma[1], Neha S. Samant[1], Maura Williams[1], Jacob B. Axelrad[1], Amiksha Shah[1], Dong Yang[1], Elizabeth A. Grimm[7], Michelle C. Barton[8], Denai R. Milton[9], Timothy P. Heffernan[10], James W. Horner[10], Suhendan Ekmekcioglu[7], Alexander J. Lazar[9], Jason Ernst[2,3,4,11,12], and Lynda Chin[1,10,13]

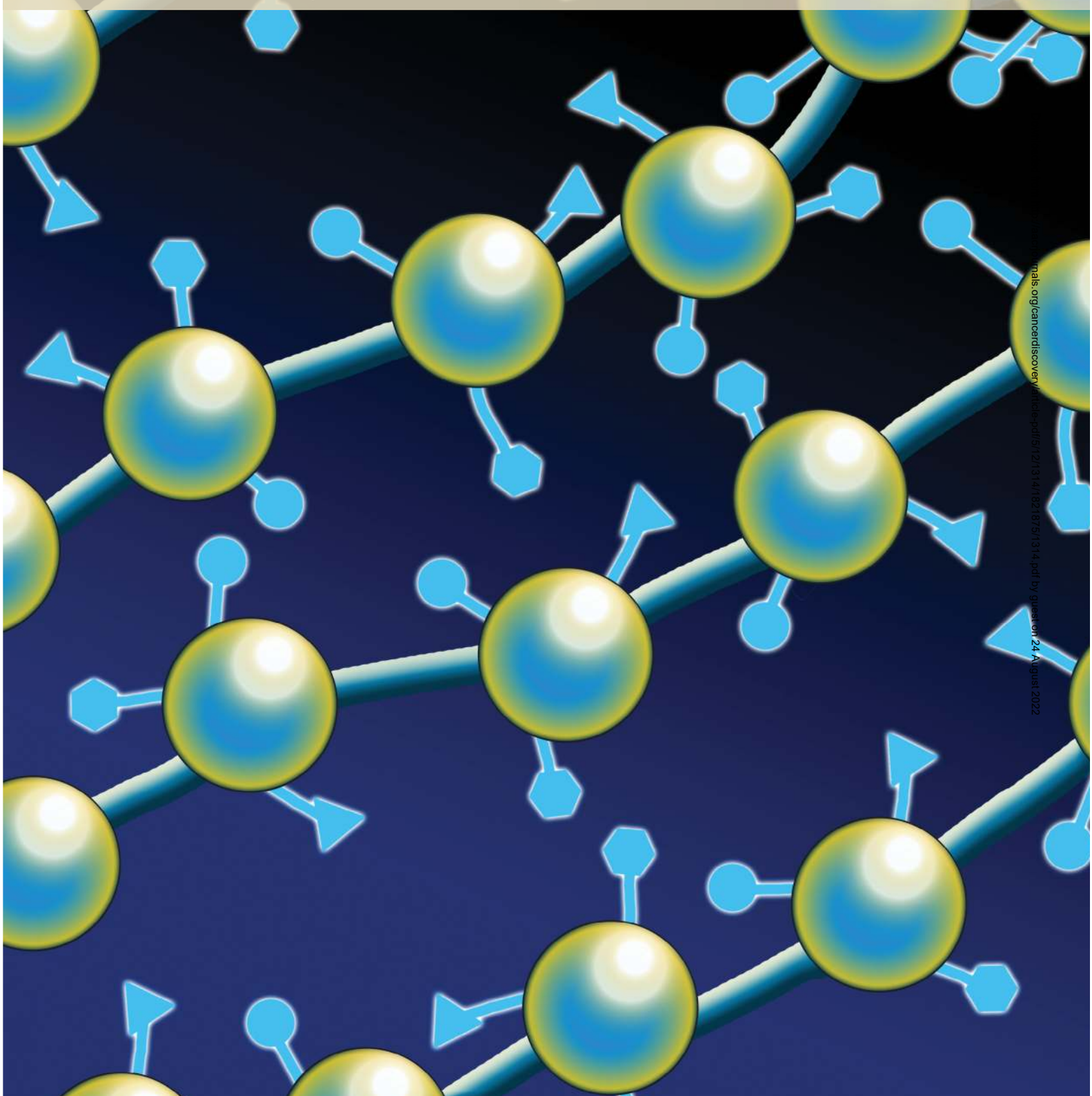

ABSTRACT Epigenetic regulators have emerged as critical factors governing the biology of cancer. Here, in the context of melanoma, we show that RNF2 is prognostic, exhibiting progression-correlated expression in human melanocytic neoplasms. Through a series of complementary gain-of-function and loss-of-function studies in mouse and human systems, we establish that RNF2 is oncogenic and prometastatic. Mechanistically, RNF2-mediated invasive behavior is dependent on its ability to monoubiquitinate H2AK119 at the promoter of *LTBP2*, resulting in silencing of this negative regulator of TGFβ signaling. In contrast, RNF2's oncogenic activity does not require its catalytic activity nor does it derive from its canonical gene repression function. Instead, RNF2 drives proliferation through direct transcriptional upregulation of the cell-cycle regulator *CCND2*. We further show that MEK1-mediated phosphorylation of RNF2 promotes recruitment of activating histone modifiers UTX and p300 to a subset of poised promoters, which activates gene expression. In summary, RNF2 regulates distinct biologic processes in the genesis and progression of melanoma via different molecular mechanisms.

SIGNIFICANCE: The role of epigenetic regulators in cancer progression is being increasingly appreciated. We show novel roles for RNF2 in melanoma tumorigenesis and metastasis, albeit via different mechanisms. Our findings support the notion that epigenetic regulators, such as RNF2, directly and functionally control powerful gene networks that are vital in multiple cancer processes. *Cancer Discov; 5(12); 1314–27. ©2015 AACR.*

See related commentary by Black and Whetstine, p. 1241.

INTRODUCTION

Epigenetic factors offer important new targets for cancer therapy given their crucial role in the regulation of major cancer-relevant transcriptional programs and their potential reversibility (1). Significant effort has been directed toward identifying key epigenetic regulators in certain cancer contexts and elucidating the specific mechanisms, cell biologic processes, and surrogate transcriptional networks governed by these factors. However, we have limited understanding of the roles of epigenetic regulators in melanoma progression.

Melanoma is an aggressive cancer with escalating incidence worldwide (2). Melanoma deaths stem primarily from widespread metastatic disease (2), though the genetic determinants and molecular mechanisms driving this disease remain poorly understood. Recent integrated genomic and functional screening efforts have identified proinvasive determinants of melanoma metastasis with potential prognostic significance (3). The list of 18 prognostic determinants that emerged from this screen was identified based on evidence of proinvasive and oncogenic capabilities *in vitro* and *in vivo*, in addition to genomic and expression alterations in human melanomas. On this list of 18, four were known epigenetic regulators: ASF1B (4), HMGB1 (5), RNF2 (6), and UCHL5 (7).

In this study, we focus on RNF2, a component of the polycomb repressor complex-1 (PRC1). RNF2 catalyzes monoubiquitination of lysine 119 of histone H2A (H2AK119ub; refs. 6, 8) and is overexpressed in gastrointestinal tumors, lymphomas, and pancreatic cancers (9, 10). However, it is not known whether RNF2 overexpression is relevant functionally and, if so, what mechanisms, biologic functions, or transcriptional networks are governed by RNF2 in a cancer context. Here, we elucidate the functional and biologic roles of RNF2 in melanoma.

RESULTS

RNF2 Is a Prognostic Metastasis Oncogene in Human Melanoma

RNF2 was previously identified as a candidate prometastasis oncogene (3). Here, we set out to validate its prometastatic and oncogenic activities and discern functional mechanisms. Metastatic function was assessed in multiple melanoma cell models, including two primary immortalized human

[1]Department of Genomic Medicine, The University of Texas MD Anderson Cancer Center, Houston, Texas. [2]Bioinformatics Interdepartmental Program, University of California, Los Angeles, Los Angeles, California. [3]Eli and Edythe Broad Center of Regenerative Medicine and Stem Cell Research at UCLA, Los Angeles, California. [4]Jonsson Comprehensive Cancer Center, University of California, Los Angeles, Los Angeles, California. [5]Department of Surgical Oncology, The University of Texas MD Anderson Cancer Center, Houston, Texas. [6]Department of Surgery, Brigham and Women's Hospital, Boston, Massachusetts. [7]Department of Melanoma Medical Oncology, The University of Texas MD Anderson Cancer Center, Houston, Texas. [8]Department of Epigenetics and Molecular Carcinogenesis, The University of Texas MD Anderson Cancer Center, Houston, Texas. [9]Department of Biostatistics, The University of Texas MD Anderson Cancer Center, Houston, Texas. [10]Institute for Applied Cancer Science, The University of Texas MD Anderson Cancer Center, Houston, Texas. [11]Departments of Biological Chemistry and Computer Science, University of California, Los Angeles, Los Angeles, California. [12]Molecular Biology Institute, University of California, Los Angeles, Los Angeles, California. [13]Institute for Health Transformation, The University of Texas System, Houston, Texas.

Note: Supplementary data for this article are available at Cancer Discovery Online (http://cancerdiscovery.aacrjournals.org/).

Corresponding Authors: Lynda Chin, The University of Texas MD Anderson Cancer Center, 1901 East Road, Rm 4SCR6.2080, Houston, TX 77054. Phone: 713-792-6876; Fax: 713-792-6806; E-mail: lchin@mdanderson.org; and Kunal Rai, 1901 East Road, Unit 1954, Houston, TX 77054; E-mail: krai@mdanderson.org

doi: 10.1158/2159-8290.CD-15-0493

melanocyte lines constitutively expressing TERT, $p53^{DD}$, $CDK4^{R24C}$, and either $BRAF^{V600E}$ or $NRAS^{G12D}$ mutant proteins (ref. 11; HMEL–$BRAF^{V600E}$ and pMEL–$NRAS^{G12D}$) and two established human melanoma cell lines, WM115 and 1205Lu. Lentiviral transduction and overexpression of wild-type RNF2 (hereafter $RNF2^{WT}$; Supplementary Fig. S1A) promoted invasion in a Boyden chamber Matrigel invasion assay in HMEL–$BRAF^{V600E}$, WM115, and 1205Lu cells (Fig. 1A; Supplementary Fig. S1B). Similarly, $RNF2^{WT}$ enhanced metastatic ability as measured by spontaneous distant metastasis (lung/liver/lymph node) in nude mice with tumor burden of 1.5 cm following intradermal injection of transduced WM115, 1205Lu, and pMEL–$NRAS^{G12D}$ cells (Fig. 1B).

To complement this approach, loss-of-function studies in the highly invasive human melanoma cell lines 501Mel (harboring high levels of RNF2; Supplementary Fig. S1C) and engineered HMEL–$BRAF^{V600E}$ melanocyte with stable shRNA targeting *PTEN* (HMEL–$BRAF^{V600E}$–sh*PTEN*) showed significant reduction in invasive potential *in vitro* upon *RNF2* knockdown with two independent shRNAs (Fig. 1C; Supplementary Fig. S1D and S1E). Because proinvasive properties are critical for seeding to distant organs during metastasis (12), we tested if RNF2 was required for seeding to distant organs. Indeed, RNF2 silencing in HMEL–$BRAF^{V600E}$–sh*PTEN* cells reduced lung seeding potential (Fig. 1D; Supplementary Fig. S1F). Furthermore, in an immunocompetent C57BL/6 host, knockdown of RNF2 in highly invasive B16-F10 cells similarly reduced lung seeding (Fig. 1E; Supplementary Fig. S1G).

Next, to explore RNF2's role as an oncogene, we assessed tumor formation following intradermal injection of $RNF2^{WT}$-overexpressing HMEL–$BRAF^{V600E}$ and pMEL–$NRAS^{G12D}$ melanocytes as well as WM115 and 1205Lu melanoma cells. $RNF2^{WT}$ significantly increased tumorigenic potential compared with control (Fig. 1F–I; Supplementary Fig. S2A–S2D) in all four cell lines tested. Similar activity of $RNF2^{WT}$ was observed in cell-based soft-agar colony formation assays, a surrogate for tumorigenesis (Fig. 1J). Reciprocally, shRNA-mediated knockdown of *RNF2* in highly tumorigenic 501Mel and WM983B cells, which express high levels of RNF2 (Supplementary Fig. S1C), resulted in a significant reduction in tumor burden (Fig. 1K; Supplementary Fig. S2E–S2G). Consistently, proliferation defects were seen in 501Mel, HMEL–$BRAF^{V600E}$–sh*PTEN*, and B16-F10 cells upon RNF2 knockdown (Supplementary Fig. S2H–S2J).

To substantiate the relevance of RNF2 in human melanoma, we verified that RNF2 expression correlates with disease progression at the mRNA and protein levels. Specifically, as summarized in Supplementary Fig. S3A, *RNF2* mRNA expression was elevated in primary melanoma tissue compared with skin and nevi (13) and, in an independent cohort, was significantly higher in metastatic lesions when compared with localized primary tumors (Supplementary Fig. S3B). Correspondingly, tissue microarray (TMA) analysis verified progression-correlated expression across 480 cores derived from 170 patients (132 benign nevi cores from 36 patients), 196 primary melanoma cores derived from 59 patients, 60 lymph node metastasis cores derived from 29 patients, and 92 visceral metastasis cores derived from 46 patients (Fig. 2A; Supplementary Fig. S3C). Overall, RNF2 expression was low in normal skin cells, including melanocytes, and progressively increased from nevi to primary melanomas to lymph node metastases.

Leveraging the clinically annotated multidimensional dataset on melanoma generated by The Cancer Genome Atlas (TCGA) Network (14 2013-04-06), we investigated the relationship between RNF2 copy number and expression correlation with cumulative overall survival. Of the 268 samples with copy-number and expression data, we found copy-number gains of *RNF2* in 42 samples (15.7%, defined by segmented copy-number value greater than 0.5), copy-number loss in 6 samples (2.2%, defined by copy-number value less than 0.5), and overexpression of RNF2 in 13 of 268 tumors (4.9%, defined by normalized expression *z* scores greater than 2). Overall, 44 tumors showed copy-number gain or overexpression of RNF2 with overlap of 11 samples ($P = 2.5e{-}8$, Fisher exact test), whereas 218 tumors showed neither copy-number change nor expression difference (hereafter referred to as "RNF2 normal"). Further, we found that amplification/overexpression of RNF2 significantly co-occurred with *NRAS* mutations (OR = 3.2; $P = 0.00077$) and was significantly mutually exclusive with *BRAF* mutations (OR = 0.37; $P = 0.0046$). Survival intervals from date of specimen submission to patients' death or last follow-up were available in 154 cases. Among these 154 cases, we found that, indeed, elevated RNF2 levels were associated with poorer overall survival (log-rank P value < 0.0039; Fig. 2B), confirming the prognostic significance of RNF2 in melanoma.

RNF2 Has Both Catalytic-Dependent and Catalytic-Independent Activities

Given RNF2's known transcriptional repressor and catalytic activities, we sought to determine whether RNF2's catalytic activity is required for its proinvasion and protumorigenic phenotypes. Mutant forms of RNF2: $RNF2^{I53S}$ and $RNF2^{R70C}$, shown previously to lack catalytic activity (15, 16), were engineered. We found that as expected, these mutants showed diminished invasion and metastasis activity compared with $RNF2^{WT}$ (Fig. 1A and B; Supplementary Fig. S1A and S1B). However, to our surprise, both $RNF2^{I53S}$ and $RNF2^{R70C}$ mutants retained the capacity to enhance proliferation and anchorage-independent growth *in vitro*, and tumorigenicity *in vivo*, at levels comparable with $RNF2^{WT}$ in all four melanoma/melanocytic cell models (Fig. 1F–J; Supplementary Figs. S2A–S2D and S3D). This observation suggested that RNF2's protumorigenic potential does not require its catalytic activity. To verify this, we performed rescue experiments with vectors encoding the open reading frames of wild-type and catalytic mutants of RNF2 in WM983B cells wherein *RNF2* was silenced with a 3′ untranslated region–directed shRNA. Consistent with the overexpression data in HMEL–$BRAF^{V600E}$ cells, $RNF2^{WT}$ and $RNF2^{I53S}$ expression were similarly able to restore soft-agar colony formation ability (Fig. 2C; Supplementary Fig. S3E).

To address the possible confounding effect of endogenous RNF2 expression in the above study, we engineered a mouse line bearing a conditional *RNF2* knockout allele with LoxP sites flanking exon 2 (Supplementary Fig. S3F), where Cre-mediated recombination results in the loss of RNF2 protein expression (Fig. 2D). The $RNF2^{L/L}$ allele was introduced into an inducible melanoma model called inducible *Braf Ink/Arf Pten* (iBIP), which harbors the following alleles: *Ink4a/Arf* $^{-/-}$, *Tyr-Cre*^{ERT2}, *Rosa26-LoxP-Stop-LoxP-Rtta, TetO-Braf*^{V600E}, and $Pten^{L/L}$ (17). The iBIP mouse model allows temporal and spatial control of tumor development and growth through

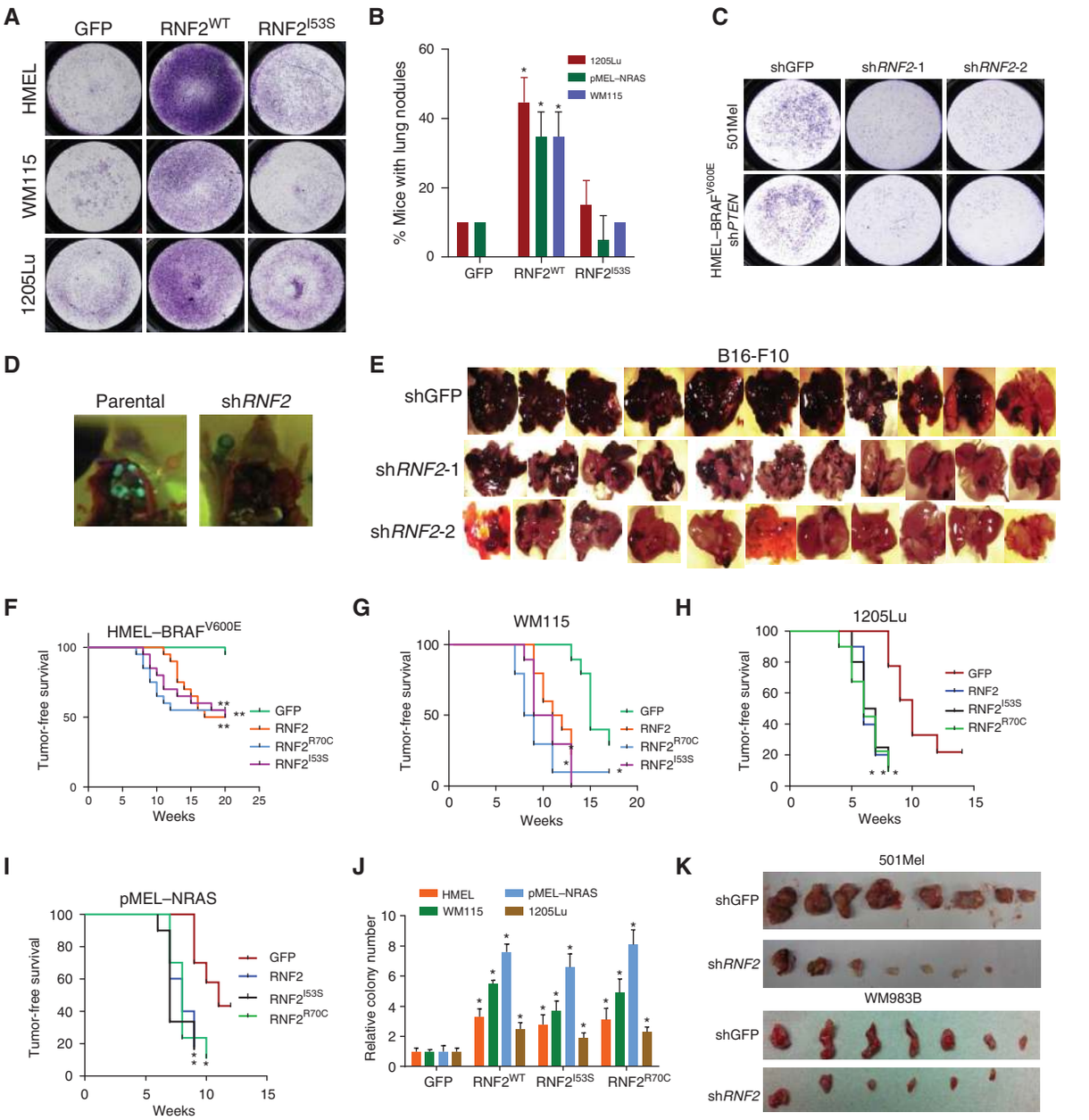

Figure 1. RNF2 overexpression promotes invasion and metastasis in a catalytic activity–dependent manner. **A,** RNF2 overexpression promotes invasion in multiple melanocytic and melanoma-derived cell lines in a catalytic activity–dependent manner. GFP, RNF2^{WT}, or RNF2^{I53S} were overexpressed by lentiviral transduction in HMEL–BRAF^{V600E} (primary melanocytes), WM115, and 1205Lu cells, and invasion capacity was measured using the Boyden chamber Matrigel invasion assay. Representative image of invasive cells is shown. pMEL–NRAS^{G12D} cells were not tested in invasion assay due to high background. **B,** RNF2 overexpression promotes metastasis. Percentage of mice with lung nodules (at the time of euthanasia due to tumor burden) is shown in the graph. HMEL–BRAF^{V600E} cells were not used in the metastasis assay due to high latency. (*, significant change *t* test $P < 0.05$). **C,** 501Mel and HMEL–BRAF^{V600E}–sh*PTEN* cells with stably integrated shGFP, sh*RNF2*-1, and sh*RNF2*-2 were subjected to Boyden chamber Matrigel invasion assay. Representative images of invaded cells are shown. **D,** representative image showing lung seeding of HMEL–BRAF^{V600E}-sh*PTEN* cells alone or with sh*RNF2*. Cells are labeled with GFP and hence the lung seeding noted by green nodules in the lung. **E,** B16-F10 mouse cells with stably integrated shGFP, sh*RNF2*-1, or sh*RNF2*-2 were injected intravenously in C57BL/6 mice. Mice were sacrificed after 16 days and lung seeding noted by color of black melanocytes in lung. **F–I,** Kaplan–Meier curve showing tumor-free survival of mice following intradermal injection of (**F**) HMEL–BRAF^{V600E} cells, (**G**) WM115 cells, (**H**) 1205Lu cells, and (**I**) pMEL–NRAS^{G12D} overexpressing GFP, RNF2 wild-type or catalytic mutant derivatives (R70C or I53S). Mantel–Cox *P* values for graph comparisons between GFP and individual RNF2 derivatives are as follows: HMEL–BRAF^{V600E} = $P < 0.005$; WM115 = $P < 0.01$; 1205Lu = $P < 0.01$; pMEL–NRAS^{G12D} = $P < 0.01$. *, $P < 0.01$ and **, $P < 0.005$. **J,** graph showing relative colony number from a soft-agar colony formation assay in HMEL–BRAF^{V600E}, pMEL–NRAS^{G12D}, WM115 cells, and 1205Lu cells overexpressing GFP, RNF2 wild-type or catalytic mutant derivatives (R70C or I53S). *, significant change *t* test $P < 0.05$. **K,** 501Mel or WM983B cells stably expressing shGFP or sh*RNF2* were subjected to tumor formation assay by intradermal injection in immunodeficient mice. Image shows subcutaneous tumors 8 weeks after injection.

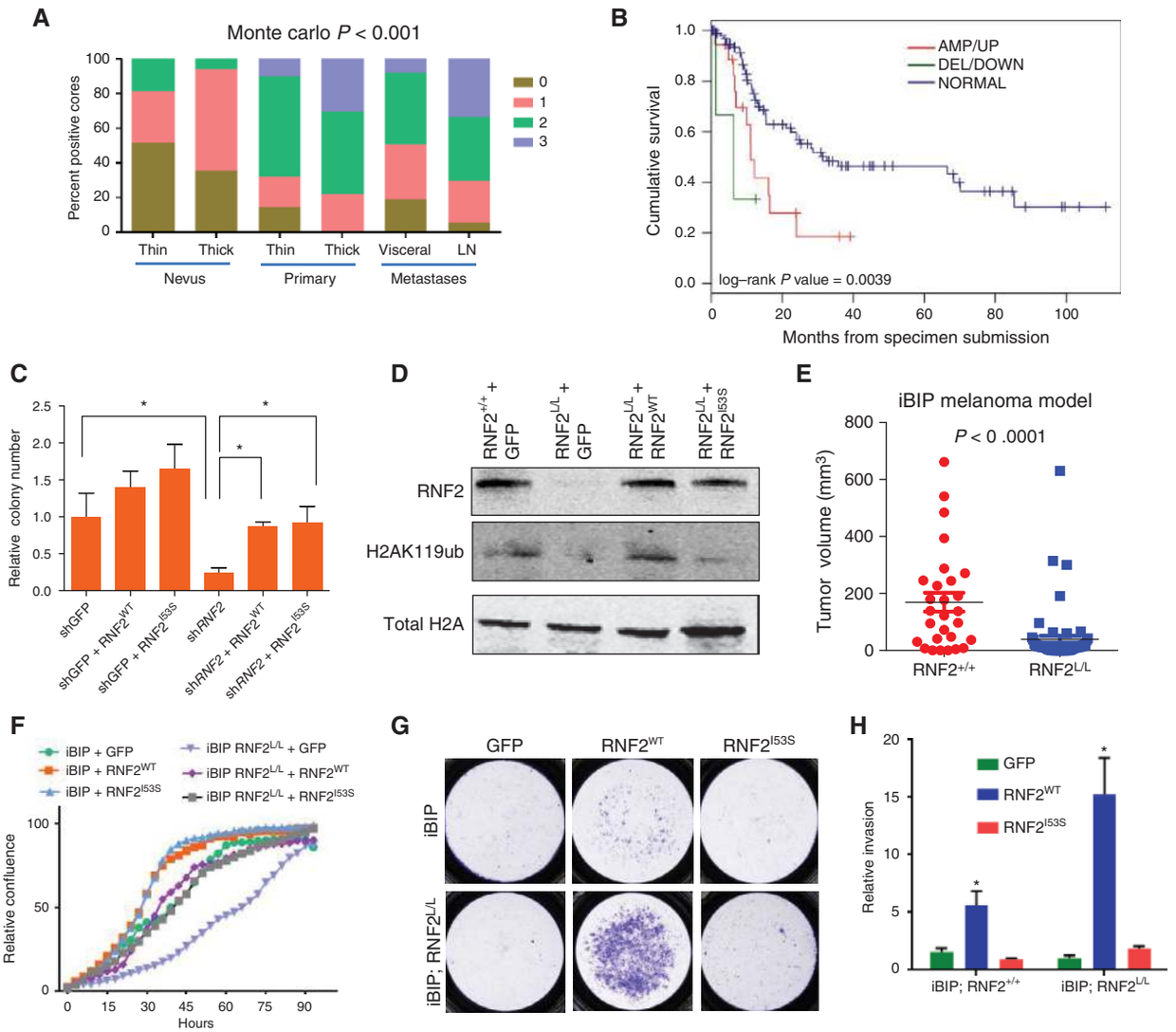

Figure 2. RNF2 promotes tumorigenesis in a catalytic activity–independent manner. **A,** bar plot showing distribution of RNF2 immunoreactive intensity counts (0, 1, 2, 3) in nevi (thin and thick), primary (thin and thick), and metastasis [visceral and lymph node (LN)]. **B,** Kaplan–Meier curve showing cumulative survival of three groups of patients defined by copy-number change and expression in a TCGA cohort with available survival data (108): amplified/upregulated (AMP/UP, 12/18, red), deleted/downregulated (DEL/DOWN, 2/4, green), and no copy-number/expression change ("Normal", 44/104, blue). **C,** graph shows relative number of soft-agar colonies in WM983B cell rescues with GFP, RNF2 wild-type or catalytic mutant derivatives (R70C or I53S; *, significant change *t* test $P < 0.05$). **D,** Western blot showing levels of RNF2, H2AK119ub, and total H2A in iBIP tumor cells with ($RNF2^{+/+}$) or without ($RNF2^{L/L}$) RNF2 overexpressing GFP, $RNF2^{WT}$, and $RNF2^{I53S}$. **E,** scatter plot showing ear tumor volume in iBIP mice with iBIP;$RNF2^{+/+}$ or iBIP;$RNF2^{L/L}$ genotype after doxycycline (2 mg/mL) administration and treatment with 4-hydroxytamoxifen (1 μmol/L). *t* test $P < 0.0001$. **F–H,** proliferation assay (**F**), invasion assay images (**G**), and (**H**) invasion assay quantitation in iBIP tumor cells with ($RNF2^{+/+}$) or without RNF2 ($RNF2^{L/L}$) overexpressing GFP, $RNF2^{WT}$, and $RNF2^{I53S}$. *, significant change *t* test $P < 0.05$.

melanocyte-specific, doxycycline-dependent *Braf*^{V600E} activation, restricted to the same cells as those undergoing 4-hydroxytamoxifen (OHT)–dependent *Pten* deletion in the *Ink4a/Arf* germline knockout background. Comparison of melanoma tumor burden following topical 4-OHT application in littermate iBIP;$RNF2^{+/+}$ and iBIP;$RNF2^{L/L}$ mice showed that RNF2 deficiency was associated with significant reduction in tumor burden at 14 weeks and improved survival (Fig. 2E; Supplementary Fig. S3G).

Using this genetic system in which *Rnf2* can be rendered homozygous null, we reassessed the differential requirement of RNF2 catalytic activity in cellular proliferation and invasion. Specifically, melanoma cells derived from iBIP; $RNF2^{L/L}$ animals were transduced with lentivirus encoding $RNF2^{WT}$ and $RNF2^{I53S}$ (Fig. 2D) and assayed for proliferation and invasion along with the levels of H2AK119ub mark. Consistent with the studies above, RNF2 catalytic activity was dispensable for proliferation enhancement yet required for invasion (Fig. 2F–H). Taken together, these *in vitro* and *in vivo* functional assays suggested that, unlike its metastatic function, RNF2's oncogenic potential is not dependent on its catalytic activity.

RNF2 Promotes TGFβ Signaling via Downregulation of LTBP2

To explore the mechanistic basis of RNF2's cancer-relevant activities, transcriptome profiling (Supplementary Fig. S4A) and ChIP-seq (chromatin immunoprecipitation followed by deep sequencing, performed using V5 antibody) occupancy profiling were performed in HMEL–BRAF^{V600E} melanocytes with enforced expression of RNF2^{WT} (hereafter HMEL–BRAF^{V600E}–RNF2^{WT}). These RNF2 ChIP-sequencing studies were also conducted in primary tumor cells derived from HMEL–BRAF^{V600E}–RNF2^{WT} melanocytes. ChIP-sequencing data analysis showed RNF2-occupied loci exhibited significantly higher enrichment of RNF2 compared with input (Supplementary Fig. S4B) and were evolutionarily conserved among 44 species (Supplementary Fig. S4C). Analyses of the distribution of RNF2 occupancy sites in relation to transcription start sites (TSS) revealed 3,465 genes in +/−5 Kb vicinity of the RNF2 occupied loci in HMEL–BRAF^{V600E}–RNF2^{WT} melanocytes (Supplementary Fig. S4D and S4E; Supplementary Table S1). Overlap of expression and occupancy datasets showed that 363 genes, whose promoters were occupied by RNF2 in HMEL–BRAF^{V600E}–RNF2^{WT} melanocytes, exhibited altered gene expression upon RNF2^{WT} overexpression compared with GFP in HMEL–BRAF^{V600E} cells (Fig. 3A; Supplementary Table S2). Although 47% of these genes with RNF2 occupancy were found to have decreased expression (compared with GFP) consistent with the classic repressive function of the RNF2–polycomb complex, it is worth noting that 53% of RNF2-occupied genes showed increased expression pointing to a likely role for RNF2 in transcriptional activation (see Discussion; Fig. 3A).

Pathway enrichment analysis of RNF2-occupied genes with increased expression showed enrichment in proliferation pathways, in addition to nucleotide synthesis and hypoxia pathways (Supplementary Fig. S4F, top 5 pathways shown), whereas RNF2-occupied genes with decreased expression are associated with regulation of transcription and nucleotide synthesis (Supplementary Fig. S4G, top 5 pathways shown). Among the RNF2-occupied genes exhibiting the most robust alterations in expression were those linked to TGFβ signaling (Fig. 3B), in line with the known role of TGFβ in invasion and metastasis (18). Thus, we next sought to determine whether RNF2 could modulate TGFβ pathway activation. First, we showed that, indeed, overexpression of RNF2^{WT}, but not RNF2^{I53S}, enhanced luciferase reporter activity driven by a generic TGFβ-responsive promoter in HEK293 cells (Fig. 3C; Supplementary Fig. S4H) and drove increased expression of TGFβ target genes (*ID1*, *ID2*, and *ID3*) in HMEL–BRAF^{V600E} melanocytes (Supplementary Fig. S4I). Consistent with a functional role of RNF2-driven TGFβ pathway activation in invasion, treatment of RNF2-overexpressing cells with an inhibitor of the TGFβ pathway (LY2157299; ref. 19) resulted in reduced invasion in Boyden chamber Matrigel invasion assays (Fig. 3D).

To identify candidate direct targets of RNF2 that govern TGFβ pathway activation, gene expression and promoter occupancy profiles were overlaid to define 363 genes (Fig. 3A), among which one of the most significantly changed genes was *LTBP2* (Fig. 3E; Supplementary Table S2), which encodes a member of the latent TGFβ binding family of proteins that resides in the extracellular matrix and regulates bioavailability of TGFβ ligand (20) to positively or negatively influence TGFβ signaling (21). This finding gains added significance because LTBP2 is downregulated upon RNF2 overexpression and has been shown previously to inhibit the migration capacity of human melanoma cells (22). Thus, we next performed ChIP–qPCR to examine the *LTBP2* promoter for occupancy by RNF2 in accordance with histone H2AK119ub modification. As shown in Fig. 3F, although the *LTBP2* promoter was occupied by RNF2 in RNF2^{WT}, RNF2^{R70C}, and RNF2^{I53S} expressing HMEL–BRAF^{V600E} melanocytes, the H2AK119ub mark was observed only in RNF2^{WT}, not RNF2^{R70C} or RNF2^{I53S}, expressing cells. In other words, the catalytic-dead RNF2 was defective in catalyzing H2AK119ub, and RNF2 enzymatic activity is not required for RNF2 binding at the promoter of *LTBP2*. Consistent with RNF2 catalytic activity–dependent repression, quantitative RT-PCR confirmed downregulation of *LTBP2* mRNA in RNF2^{WT}, but not RNF2^{R70C} or RNF2^{I53S}, expressing cells (Fig. 3G). This was also validated in the human melanoma cell lines 501Mel and WM983B, where we noted RNF2 occupancy in parental cells and loss of H2AK119ub signal in 501Mel and WM983B cells upon RNF2 knockdown (Fig. 3H and I). Consistently, activating histone acetylation marks were enriched on the *LTBP2* promoter (Fig. 3H and I), and its mRNA expression was increased upon RNF2 knockdown (Fig. 3J). In addition, LTBP2-mediated modulation of TGFβ signaling is supported by the correlation of LTBP2 knockdown with upregulation of the TGFβ target genes *ID1*, *ID2*, and *ID3* (Fig. 3K; Supplementary Fig. S4J), as well as with enhanced invasion activity *in vitro* (Fig. 3L). Finally, the functional epistatic link between RNF2 and LTBP2 is supported by the demonstration that LTBP2 overexpression partially inhibited the invasive activity of RNF2^{WT}-overexpressing melanocytes (Fig. 3M and N).

RNF2 Promotes Tumorigenesis through Upregulation of CyclinD2

As noted above, many genes proximal to RNF2 occupancy sites in HMEL-RNF2^{WT} melanocytes showed increased expression (Fig. 3A). Indeed, the most significantly upregulated and occupied gene was *CCND2*, which encodes the cell-cycle regulator Cyclin D2 (Fig. 4A; Supplementary Table S2). ChIP–qPCR confirmed RNF2 occupancy at the *CCND2* promoter in HMEL–BRAF^{V600E} cells overexpressing RNF2^{WT}, RNF2^{R70C}, and RNF2^{I53S} (Fig. 4B). In addition, CCND2 expression was induced by ectopic RNF2 (wild-type or catalytic dead) and remained high in HMEL–BRAF^{V600E} cells overexpressing RNF2^{WT}, RNF2^{R70C}, and RNF2^{I53S} (Fig. 4C), suggesting that transcriptional activation did not require catalytic activity or histone H2AK119 ubiquitination. Indeed, no enrichment of the H2AK119ub mark was detected on the *CCND2* promoter (Fig. 4B), which instead possessed activating chromatin modifications, including H3K9ac, H3K27ac, H4TetraAc, and H3K4me3, in HMEL–BRAF^{V600E} cells overexpressing both wild-type and catalytic mutants of RNF2 (Fig. 4B). Accordingly, RNF2 knockdown caused repression of CCND2 expression (Fig. 4D) and removal of activation marks in WM983B and 501Mel cells (Fig. 4E and F).

To assess the potential role of RNF2-directed CCND2 upregulation in promoting increased proliferation and tumorigenesis,

A

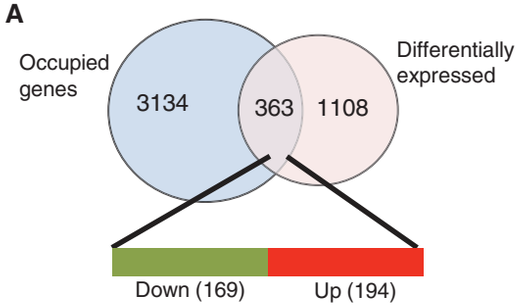

B

Upstream regulator	*P*-value of overlap
TNF	1.93E–08
TGFβ1	6.44E–07
MYCN	1.46E–06
ARNT	2.16E–06
CEBPα	2.39E–06

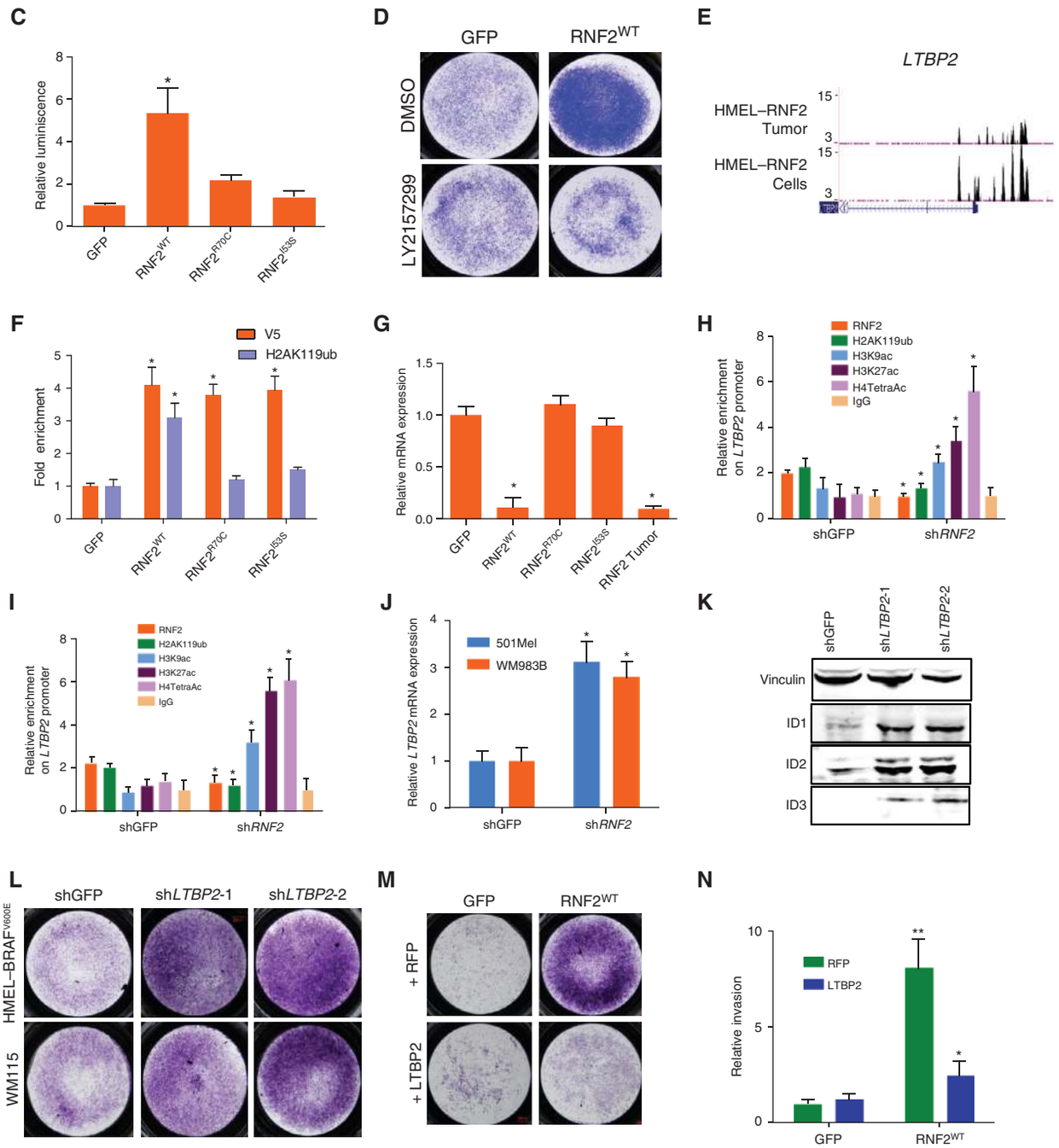

shRNA-mediated knockdown of *CCND2* was performed in HMEL–BRAF^{V600E}–RNF2^{WT}-overexpressing cells (Fig. 4G). As shown in Fig. 4H–J, *in vivo* tumor formation (Fig. 4H), enhancement in two-dimensional proliferative capacity (Fig. 4I), and three-dimensional anchorage-independent growth (Fig. 4J) conferred by RNF2^{WT} overexpression were partially reversed upon CCND2 knockdown, suggesting that CCND2 contributes to pro-oncogenic activities of RNF2. Consistently, knockdown of CCND2 reduced the proliferative capacity of 501Mel and WM983B cells, which express high levels of RNF2 (Fig. 4K).

Preexisting Chromatin Promoter States Determine the Genes Activated by RNF2

Next, we sought to understand how RNF2 might promote gene activation contrary to its known role in gene repression. We considered the possibility that the transcriptional fate of genes regulated by RNF2 might depend on the chromatin states that preexisted on their promoters before upregulation of RNF2. To identify these preexisting chromatin states of RNF2-regulated genes in melanocytes before RNF2 overexpression, we performed epigenomic analyses for 35 histone marks in the HMEL–BRAF^{V600E} cell system that was used in the RNF2 gain-of-function experiments (Rai and colleagues, unpublished data). There, we modeled histone modification profiles as 45 defined chromatin states using the ChromHMM modeling method (ref. 23; see Methods; Fig. 5A), which captures important biologic states such as poised or bivalent promoter/enhancer states (state 26 and state 6; ref. 24). Each of these chromatin states was annotated based on the enrichment of different histone marks as well as the enrichment of known genomic elements (Fig. 5A; Supplementary Fig. S5A–S5B; Supplementary Table S3). We overlapped RNF2 binding sites to these chromatin states and found that, although all RNF2 binding sites in the genome overlapped with a number of states, the sites that were associated with genes showing altered expression were limited to promoter and poised states (Fig. 5A). Interestingly, we noted that promoters of the genes upregulated by RNF2, including *CCND2*, were specifically enriched in state 26, whereas RNF2-downregulated promoters were markedly absent (Fig. 5A). These downregulated promoters displayed only active promoter states (states 1–3, 5). Therefore, we compared the cumulative presence of H3K27me3 marks on all upregulated and downregulated RNF2-bound promoters. As shown in Fig. 5B, H3K27me3 was significantly enriched at promoters that are upregulated by RNF2, compared with promoters of genes destined for repression by RNF2 that lack enrichment of this mark. Consistent with this, a UCSC genome browser view of the *CCND2* promoter showed prominent peaks of H3K27me3 and H3K4me3, characteristic of state 26 (poised enhancer/promoter) and state 6 (poised promoter), around RNF2 binding sites immediately upstream of the TSS (Fig. 5C). In contrast, analysis of the *LTBP2* promoter, which is repressed when RNF2 is expressed, showed enrichment of active promoter states (states 1 and 2) and active promoter marks (H3K4me3 and H3K9ac) as well as enhancer states (states 7, 8, and 9) and enhancer (H3K27ac) marks (Fig. 5D). These data suggest that genes activated by RNF2 may be marked, or poised, by the repression-associated mark H3K27me3 prior to RNF2-mediated activation and gain of histone acetylation marks.

RNF2 Recruits UTX and p300 to the *CCND2* Promoter

Recently, MLL2, UTX, and p300 were identified as RNF2-associated proteins in mouse ES cells, which co-migrate on a sucrose gradient separately from RNF2-containing PRC1 components (25). This observation suggests that a fraction of RNF2 molecules may exist in an activating complex with MLL2, UTX, or p300. Therefore, we hypothesized that a subfraction of RNF2 may preferentially recruit activating factors to the H3K27me3-containing poised promoters. To investigate this, we first tested whether RNF2 overexpression led to H3K27me3 loss on activated promoters. Indeed, RNF2 overexpression led to loss of H3K27me3 occupancy as well as gain of histone acetylation marks (H3K9ac, H3K27ac, and H4TetraAc) on the *CCND2* promoter (Figs. 6A and 4B). These histone modification events upon RNF2 overexpression were consistent with RNF2's suggested interaction with UTX, an H3K27 demethylase, and p300, a histone acetyltransferase (25). Indeed, ChIP–qPCR showed that UTX and p300 were enriched on the *CCND2* promoter after RNF2 overexpression (Fig. 6B). Consistent with these observations, we noted interactions between RNF2 and UTX by coimmunoprecipitation in HMEL–BRAF^{V600E}–RNF2^{WT} cells (Fig. 6C). Finally, we tested whether *UTX* and *p300* recruitment by RNF2 had any impact on transcriptional activation of the *CCND2* promoter. Downregulation of UTX or p300 individually by shRNAs significantly reduced CCND2 expression in RNF2-overexpressing cells but not in control cells (Fig. 6D). Together, these observations suggest that recruitment of UTX and p300 to the *CCND2* promoter by RNF2 is critical for creating an activating chromatin environment as well as transcriptional activation.

Figure 3. RNF2 promotes TGFβ signaling. **A,** overlap of genes with corresponding promoters occupied by RNF2 (using ChIP-Seq data) and differentially expressed genes. As many as 363 genes show overlap, of which 169 (47%, green) are downregulated and 194 (53%, red) are upregulated. **B,** top 5 pathways from upstream regulating factor enrichment by Ingenuity Pathway Analysis (IPA). Note that TGFβ target genes were one of the most significantly deregulated and occupied genes. **C,** luciferase assay showing increased TGFβ-responsive promoter activity in HEK293 cells with overexpression of RNF2^{WT}, but not with RNF2^{R70C} and RNF2^{I53S}. **D,** representative image from a Boyden chamber Matrigel invasion experiment in HMEL–BRAF^{V600E} cells overexpressing GFP or RNF2^{WT} and treated with DMSO or LY2157299 (TGFβRI inhibitor). Invaded cells stained with crystal violet are shown. **E,** occupancy of RNF2 on the *LTBP2* promoter. Two ChIP-Seq tracks are shown: top: HMEL–BRAF^{V600E}–RNF2^{WT} tumor cells; bottom: HMEL–BRAF^{V600E}–RNF2^{WT} cells. **F–G,** (**F**) qPCR validation showing enrichment of V5-RNF2 (V5 antibody) and H2AK119ub on *LTBP2* promoter and (**G**) mRNA expression of *LTBP2* in HMEL–BRAF^{V600E} cells overexpressing GFP, RNF2 wild-type or catalytic mutant derivatives (R70C and I53S). **H** and **I,** graph shows relative occupancy enrichment of RNF2 (endogenous), H2AK119ub, H3K9ac, H3K27ac, H4TetraAc, and IgG on *LTBP2* promoter as obtained by ChIP-qPCR in shGFP or sh*RNF2*-infected 501Mel (**H**) and WM983B (**I**) cells. **J,** relative mRNA expression of *LTBP2* in shGFP or sh*RNF2*-infected 501Mel or WM983B cells. **K,** Western blot showing protein levels of TGFβ target genes ID1, ID2, and ID3 in HMEL–BRAF^{V600E} cells with knockdown of *LTBP2* using two shRNAs. **L** and **M,** representative image of invaded cells from a triplicate Boyden chamber Matrigel invasion experiment in (**L**) HMEL–BRAF^{V600E} or WM115 cells with knockdown of *LTBP2* using two shRNAs and (**M**) HMEL–BRAF^{V600E} cells overexpressing GFP or RNF2^{WT} along with either RFP or LTBP2. **N,** graph showing quantitation of experiment shown in panel **M**. Across all panels, *, significant change *t* test $P < 0.05$ and **, P value < 0.01.

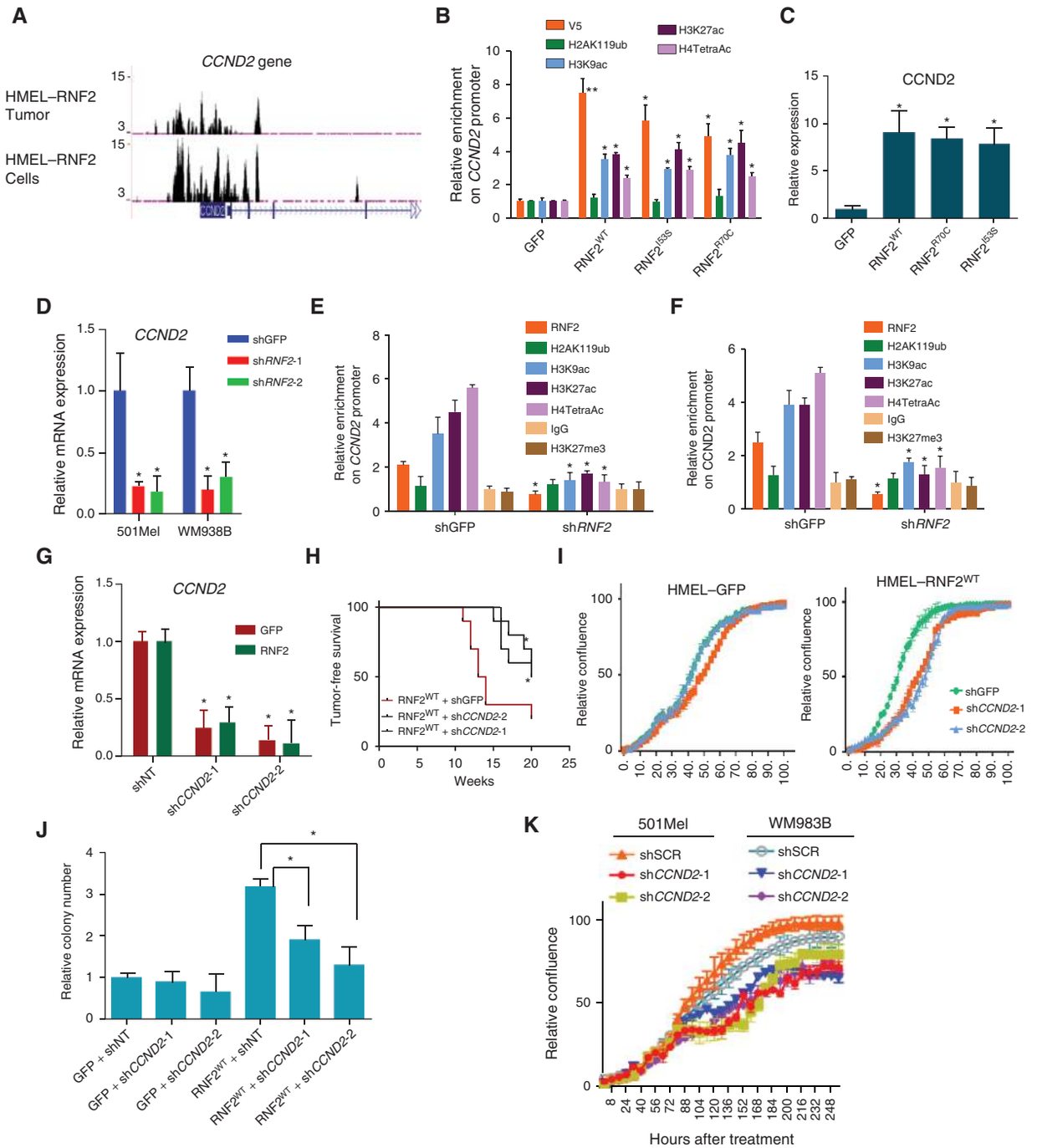

Figure 4. Oncogenic activity of RNF2 depends on upregulation of CCND2. **A,** occupancy of RNF2 on the promoter of *CCND2*. Two ChIP-Seq tracks are shown: top: HMEL-BRAF^{V600E}–RNF2^{WT} tumor cells; bottom: HMEL-BRAF^{V600E}–RNF2^{WT} cells. **B,** graph shows relative occupancy enrichment of V5 RNF2 (using V5 antibody), H2AK119ub, H3K9ac, H3K27ac, and H4TetraAc on *CCND2* promoter as obtained by ChIP-qPCR in GFP, RNF2^{WT}, RNF2^{I53S}, or RNF2^{R70C} overexpressing HMEL-BRAF^{V600E} cells. **C,** graph shows relative CCND2 expression in HMEL-BRAF^{V600E} cells overexpressing GFP, RNF2 wild-type or catalytic mutant derivatives (R70C or I53S). Values were normalized to GFP cells as 1. **D,** graph showing mRNA expression levels of *CCND2* in 501Mel and WM983B cells with RNF2 knockdown. **E** and **F,** graph shows relative occupancy enrichment of RNF2 (endogenous), H2AK119ub, H3K9ac, H3K27ac, H4TetraAc, H3K27me3, and IgG on *CCND2* promoter as obtained by ChIP-qPCR in shGFP or sh*RNF2*-infected 501Mel (**E**) and WM983B (**F**) cells. **G,** graph shows mRNA expression of *CCND2* in HMEL-BRAF^{V600E} cells with GFP or RNF2^{WT} overexpression with two stably integrated *CCND2* shRNAs. **H–J,** assays for tumorigenicity in RNF2^{WT} overexpressing HMEL-BRAF^{V600E} cells with *CCND2* knockdown (two shRNAs). **H,** Kaplan–Meier curve showing tumor-free survival (Mantel–Cox $P < 0.05$), (**I**) relative cell density from *in vitro* proliferation assay, and (**J**) soft-agar colony counts. **K,** proliferation curves for 501Mel and WM983B cells infected with shRNAs for GFP (shGFP) or *CCND2* (sh*CCND2*-1 and sh*CCND2*-2). Across all panels, *, significant change *t* test $P < 0.05$ and **, *P* value < 0.01.

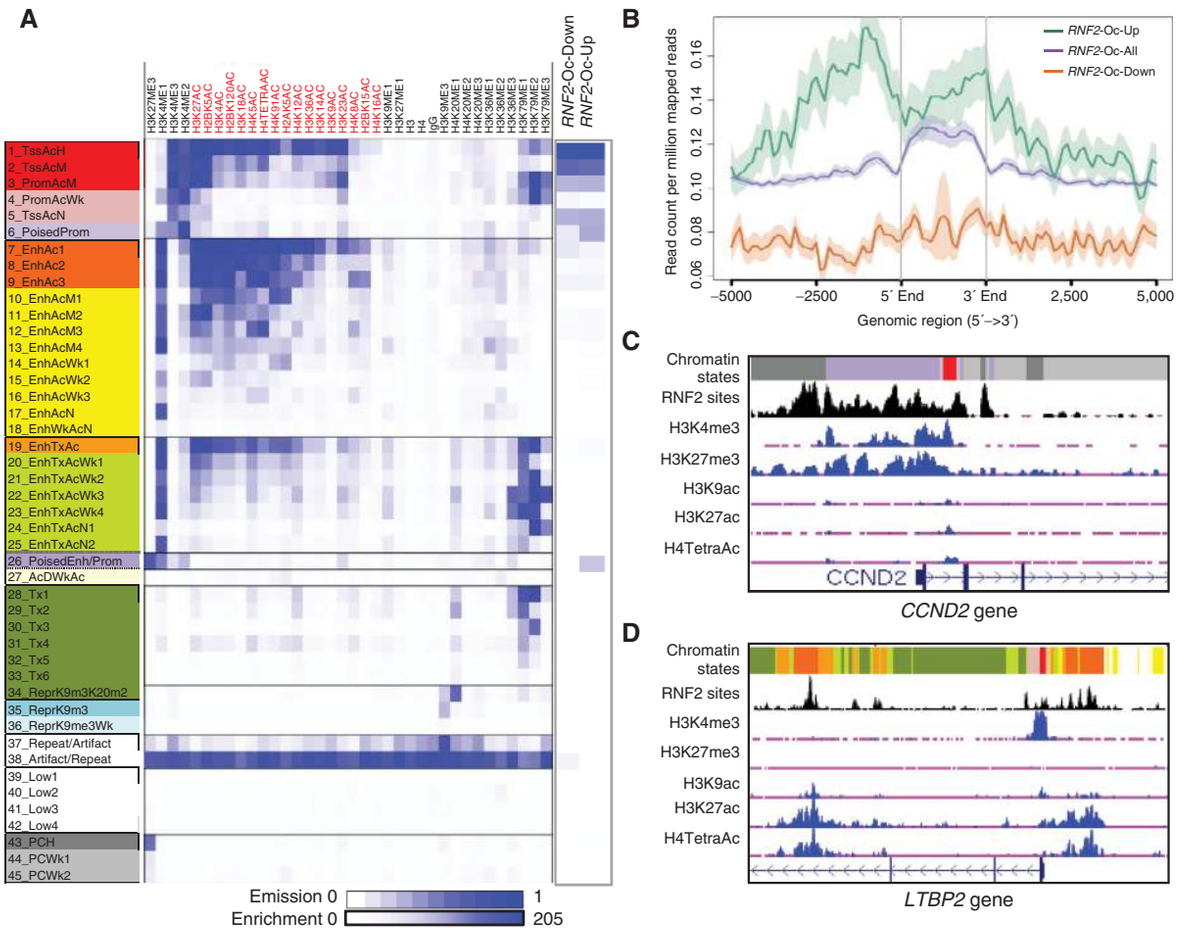

Figure 5. RNF2-activated genes harbor H3K27me3 poised chromatin state. **A,** overlap of RNF2 binding sites, upregulated and downregulated promoters with 45-state model predicted by ChromHMM of occupancy of 35-histone marks in HMEL-BRAF^{V600E} cells (data described in Rai et al., unpublished data). *X*-axis shows histone modification antibodies used for modeling; *Y*-axis shows chromatin states and description of each state (also in Supplementary Table S3). Blue is enrichment. Scale is shown at the bottom. **B,** graph showing enrichment of H3K27me3 on all genes (*RNF2*-Oc-All), upregulated genes (*RNF2*-Oc-Up), and downregulated (*RNF2*-Oc-Down) containing RNF2 binding sites in their promoters. 5′ end, 3′ end, and the distance from TSS are shown on the *X*-axis. Shadow, SEM. **C** and **D,** UCSC genome browser view of *CCND2* promoter (**C**) and *LTBP2* promoter (**D**) showing chromatin state enrichment as well as RNF2 binding sites.

MEK-Mediated Phosphorylation of RNF2

To understand how RNF2 might act as both an activator and a repressor in the same cell, we asked whether a particular modified form of RNF2 is important for gene activation. It was previously shown that RNF2 is phosphorylated in a MEK-dependent manner, and this phosphorylation may be associated with histone acetylation events (26). Because RNF2 overexpression was studied in the context of activated MAPK signaling (due to *BRAF*^{V600E} mutation), which is known to activate MEK, we asked whether phosphorylation of RNF2 by MEK may be important for its role in gene activation in the context of melanoma. We first verified that MEK1 is indeed able to phosphorylate RNF2 using an *in vitro* kinase assay (Fig. 7A). Moreover, serine 41 (26) to alanine mutant derivative of RNF2 showed significantly reduced phosphorylation compared with wild-type, whereas S168A, and S208A mutant derivatives were phosphorylated to the same extent as wild-type RNF2. Further, treatment of RNF2^{WT}-overexpressing HMEL-BRAF^{V600E} cells with the MEK inhibitor trametinib led to a significant reduction in *CCND2* gene activation by RNF2^{WT}, whereas LTBP2 expression remained unchanged and overexpression of RNF2^{S41A} failed to activate the *CCND2* promoter (Fig. 7B). Consistently, RNF2 induced H3K27me3 demethylation, H3K27ac accumulation, and UTX/p300 recruitment at the *CCND2* promoter, which were abrogated by MEK inhibition in RNF2^{WT}-overexpressing cells (Fig. 7C). In parallel, the S41A mutant was inefficient in promoting H3K27me3 demethylation and inducing H3K27ac and UTX/p300 recruitment (Fig. 7C). Consistently, MEK inhibition and the S41A mutant drastically reduced the interaction between RNF2 and UTX (Fig. 7D). Finally, we showed that MEK inhibition selectively reduces the increased proliferation conferred by RNF2 overexpression in HMEL-BRAF^{V600E}, WM115, and 1205Lu cells (Fig. 7E–G), suggesting a therapeutic strategy to suppress RNF2-mediated tumorigenesis.

Together, these data support a model wherein MEK-mediated RNF2 phosphorylation may induce its interaction with histone modifiers, such as UTX and p300, and their

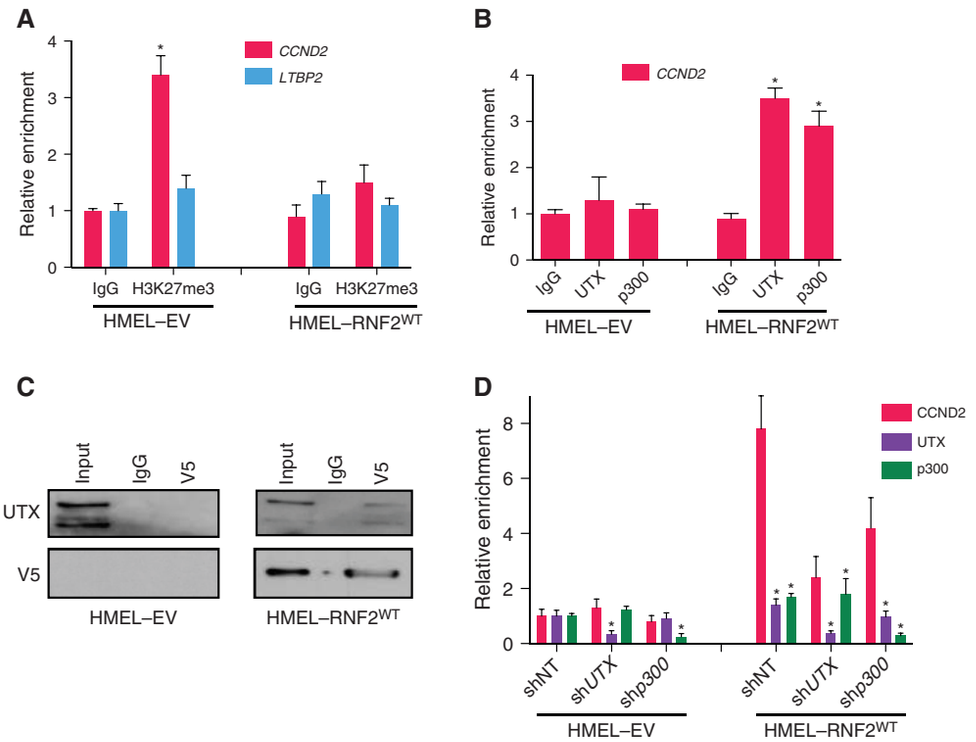

Figure 6. RNF2 recruits and requires UTX and p300 for *CCND2* activation. **A,** relative occupancy of H3K27me3 on *CCND2* and *LTBP2* promoters in HMEL-BRAF^{V600E}-EV and HMEL-BRAF^{V600E}-RNF2^{WT} cells. **B,** relative occupancy of UTX and p300 on *CCND2* promoter. **C,** Western blot showing coimmunoprecipitation of UTX upon immunoprecipitation of RNF2 (using anti-V5) from HMEL-BRAF^{V600E}-EV and HMEL-BRAF^{V600E}-RNF2^{WT} cells. **D,** relative expression of CCND2, UTX, and p300 in HMEL-BRAF^{V600E}-EV and HMEL-BRAF^{V600E}-RNF2^{WT} cells upon control (shNT), *UTX* (sh*UTX*), and *p300* (sh*p300*) knockdown. *, significant change *t* test $P < 0.05$.

recruitment to poised H3K27me3 containing promoters. This recruitment, and subsequent loss of H3K27me3 with gain of activating histone marks, selectively creates an activating environment on gene promoters that exist in a poised state.

DISCUSSION

In this study, we elucidated distinct molecular mechanisms by which RNF2 regulates proliferation and invasion, highlighting the complex and multifaceted action of epigenetic regulators. Molecularly, the intersection of RNF2 chromatin binding and gene expression analyses identified RNF2-occupied repressed and active promoters. Biologically, a series of reinforcing functional assays utilizing both somatic and genetically engineered germline model systems demonstrated that RNF2's catalytic activity is dispensable for CCND2 activation, which drives proliferation, but is required for suppression of LTBP2 and activation of TGFβ signaling for invasion and metastasis.

Although it has been suggested that RNF2 may promote gene repression by chromatin compaction independently of its catalytic activity (27), this is the first report of RNF2's role in gene activation independent of its E3 ubiquitin ligase activity. In this regard, we found that approximately 53% of genes with RNF2-occupied promoters were upregulated in RNF2-overexpressing melanocytes. As with other transcription factors, an intriguing question is how RNF2 might act as both an activator and repressor in the same cell type. A subset of genes activated by RNF2 in this study have poised promoters strongly enriched in the H3K27me3 mark as well as showing weak enrichment of activating histone acetylation and methylation marks. We provide mechanistic insights that MEK1-dependent phosphorylation of RNF2 may promote its binding to activating chromatin modifiers, such as UTX and p300, which in turn remove H3K27me3 and acetylate the promoter, respectively, to open chromatin for gene activation. MEK-dependent phosphorylation of RNF2 provides precedence for a mechanism that signaling proteins may utilize the same molecule to effect gene-specific outcomes in a context-dependent manner. Finally, our data also suggest that MEK inhibitors could be used to block RNF2's protumorigenic function and therefore could be potentially beneficial in the clinic to suppress growth of *RNF2*-amplified tumors.

TGFβ signaling has been shown to be critical for induction of proinvasion and migration genes, such as MMPs, N-cadherin, vimentin, and fibronectin. Here, we identified RNF2 as an important epigenetic regulator of TGFβ signaling. Promoter occupancy and expression analyses in this study revealed that RNF2 can directly bind to the *LTBP2* promoter to create a repressive environment through H2AK119 ubiquitination and consequent gene silencing. Although LTBP proteins have been reported to both negatively and

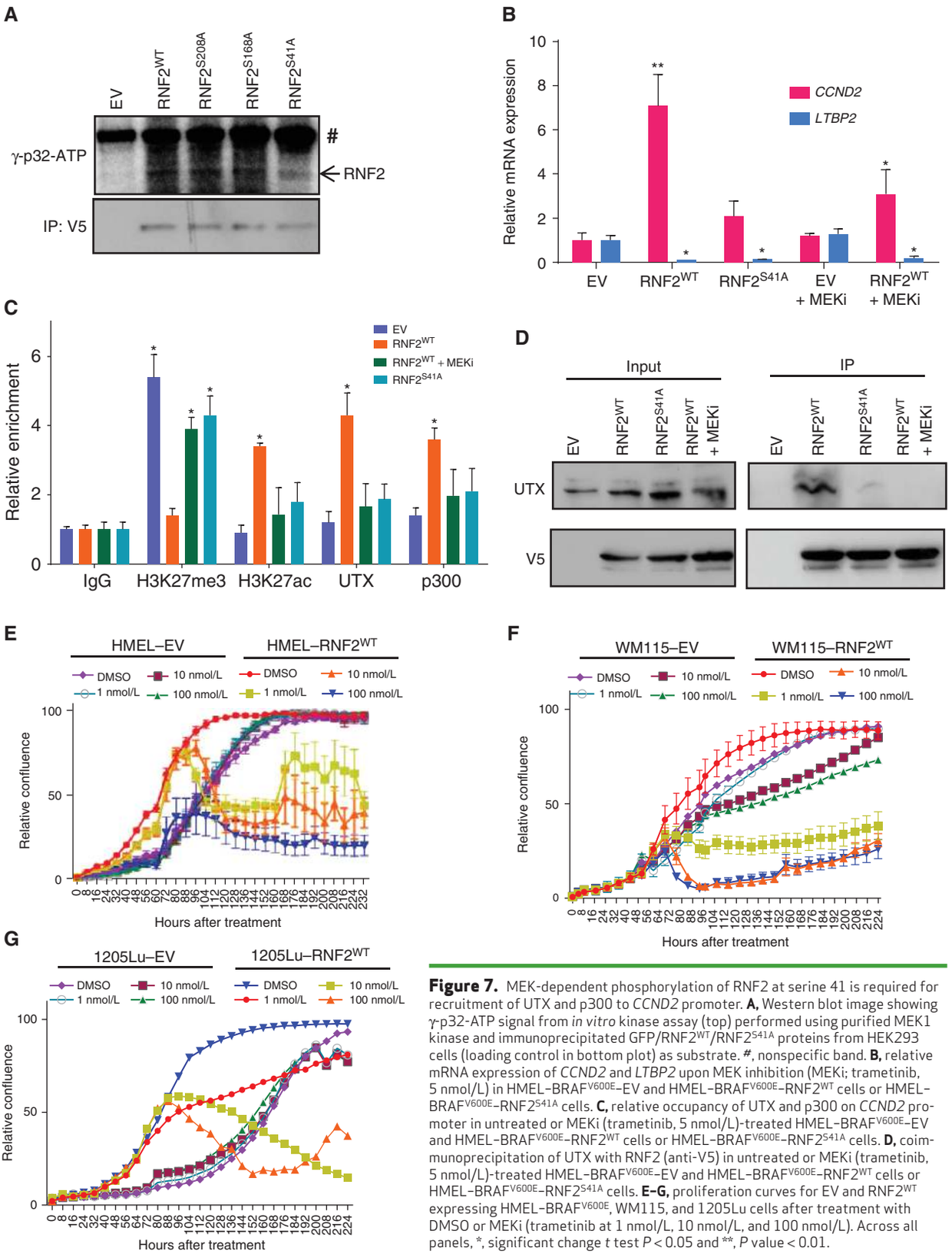

Figure 7. MEK-dependent phosphorylation of RNF2 at serine 41 is required for recruitment of UTX and p300 to *CCND2* promoter. **A,** Western blot image showing γ-p32-ATP signal from *in vitro* kinase assay (top) performed using purified MEK1 kinase and immunoprecipitated GFP/RNF2^{WT}/RNF2^{S41A} proteins from HEK293 cells (loading control in bottom plot) as substrate. **#**, nonspecific band. **B,** relative mRNA expression of *CCND2* and *LTBP2* upon MEK inhibition (MEKi; trametinib, 5 nmol/L) in HMEL-BRAF^{V600E}-EV and HMEL-BRAF^{V600E}-RNF2^{WT} cells or HMEL-BRAF^{V600E}-RNF2^{S41A} cells. **C,** relative occupancy of UTX and p300 on *CCND2* promoter in untreated or MEKi (trametinib, 5 nmol/L)-treated HMEL-BRAF^{V600E}-EV and HMEL-BRAF^{V600E}-RNF2^{WT} cells or HMEL-BRAF^{V600E}-RNF2^{S41A} cells. **D,** coimmunoprecipitation of UTX with RNF2 (anti-V5) in untreated or MEKi (trametinib, 5 nmol/L)-treated HMEL-BRAF^{V600E}-EV and HMEL-BRAF^{V600E}-RNF2^{WT} cells or HMEL-BRAF^{V600E}-RNF2^{S41A} cells. **E–G,** proliferation curves for EV and RNF2^{WT} expressing HMEL-BRAF^{V600E}, WM115, and 1205Lu cells after treatment with DMSO or MEKi (trametinib at 1 nmol/L, 10 nmol/L, and 100 nmol/L). Across all panels, *, significant change *t* test $P < 0.05$ and **, P value < 0.01.

positively regulate TGFβ signaling (20), our study suggests that, in melanoma, LTBP2 acts as a negative regulator of TGFβ signaling in invasion. We noted that apart from LTBP2, mRNA expression of the EMT transcription factor ZEB2 was also increased in RNF2-expressing cells and may also contribute to the prometastatic phenotype conferred by RNF2. Moreover, we provide strong evidence for requirement of its E3-ubiquitin ligase activity in the promotion of invasive and metastatic properties by RNF2. This, against the backdrop of the well-known opposing effect of TGFβ signaling, raises the possibility that inhibition of RNF2 catalytic activity offers a new therapeutic intervention to target the metastatic activity of TGFβ in metastatic melanoma.

An important question is whether prometastatic and protumorigenic activities of RNF2 are completely independent of each other. Although we provide evidence that the proinvasive/metastatic function is dependent on RNF2's catalytic activity and the protumorigenic role is independent of it, our data do not completely rule out the possibility that RNF2's role in proliferation also contributes to its prometastatic phenotype.

Taken together, our findings provide strong evidence that epigenetic regulators, such as RNF2, directly and functionally control powerful gene networks that are vital in multiple cancer processes.

METHODS

Cell Culture, Proliferation Assays, Soft-Agar Colony Formation Assay, and Boyden Chamber Invasion Assay

Cells were grown in standard tissue culture conditions (5% CO_2, 37°C). HMEL–$BRAF^{V600E}$ cells were a kind gift of Dr. David Fisher. 1205Lu, WM115, 501Mel, and WM983B cells were obtained from either the ATCC or Coriell and maintained according to the manufacturer's instructions. Cell lines were authenticated by short tandem repeat profiling and tested every 2 months for *Mycoplasma* contamination. Cell proliferation assays were performed using an IncuCyte instrument (Essen Bioscience). The instrument captures bright field images every 2 hours and calculates cell density based on the area occupied by cells compared with total area. Soft-agar colony formation assay was performed as described earlier (3). Briefly, two layers of soft agar (bottom layer 0.8% and top layer 0.5%) mixed with DMEM growth medium and FBS were prepared. Two thousand cells were mixed in the top agar layer during plating, and colony formation was monitored. When the colonies reached appropriate size, the colonies were stained with p-iodonitrotetrazolium violet, pictures were taken, and the colonies were counted manually or with ImageJ software. Boyden chamber Matrigel invasion assay was performed as described earlier (3). Briefly, chambers were brought to room temperature and hydrated in serum-free media. One hundred thousand cells were seeded inside the chamber in serum-free media and assayed for the ability to move to the bottom of the chamber in response to 10% serum containing media present in the well after 24 to 48 hours.

Mice Injections and Tumor Studies

Four-to-six-week-old NCR-NUDE mice were purchased from Taconic and injected intradermally with 1 million cells. Tumor volume was measured at designated time points. Mice were euthanized and tumors harvested when tumor size reached 1.5 cm. Mice were maintained in either the animal facility at the Harvard Center for Comparative Medicine or in the animal facility at The MD Anderson Cancer Center. All animal experiments were approved by an Institutional Animal Care and Use Committee review board.

TMA and Immunohistochemistry

TMA for melanoma progression has been previously described (28). RNF2 immunohistochemistry was performed using Prestige rabbit polyclonal antibody (Sigma). TMA slides were heated at 65°C for 1 hour, deparaffinized in xylene, and rehydrated. Antigen retrieval was performed by boiling at 115°C for 10 minutes and then at 95°C for 30 seconds. After cooling, slides were incubated in 3% H_2O_2 for 20 minutes, washed in PBS, and blocked in goat serum. Following incubation with primary antibody (1:200) overnight, slides were incubated in secondary antibody for 1 hour at 37°C. Slides were then washed and incubated in ABC elite reagent (Vector Labs) and developed using ImmuPACT (Novagen). Manual blinded scoring of the TMA core intensity was performed by two independent pathologists.

Chromatin Immunoprecipitation and Next-Generation Sequencing (ChIP-Sequencing)

Chromatin immunoprecipitation was performed as described earlier (29). Library preparation was done using New England BioLabs reagents as described earlier (29). Sequencing was performed in HiSeq 2000 (Illumina). Data analysis was performed as described in Supplementary Methods.

RNA Isolation, Quantitative PCR, and Microarray

RNA was isolated using the RNeasy Kit (Qiagen) per the manufacturer's instructions. cDNA was prepared using SuperScript III (Life Technologies) per the manufacturer's instructions. qPCR was performed using SybrGreenER (Invitrogen) and Stratagene instrument. Microarray experiments were performed in the MD Anderson Center for ncRNA Sequencing core facility. Microarray data were analyzed using LIMMA bioconductor package. Details of analysis are provided in Supplementary Methods. All genomic datasets are publicly available at the National Center for Biotechnology Information's Gene Expression Omnibus database (GSE51928, GSE51929, and GSE51930).

Survival Analysis in TCGA Data

TCGA melanoma data (2013_04_06 stddata run) were retrieved from the Genome Data Analysis Center of the TCGA. Survival intervals from date of specimen submission to patients' death/last follow-up were available in 154 cases. Statistical significance of survival differences was estimated by Kaplan–Meier curves and log-rank test in R.

Protein Isolation and Western Blotting

Proteins were made using RIPA buffer (Boston BioProducts) and complete mini protease inhibitor cocktail (Roche). Western blotting was performed by standard procedure using Invitrogen or Bio-Rad precast 4% to 12% gels. Antibodies used were anti-V5 (Invitrogen), anti-vinculin (Sigma), anti-H2AK119ub (Millipore), anti-RNF2 (Sigma), anti-ID1 (SCBT), anti-ID2 (SCBT), anti-ID3 (SCBT). Secondary antibodies used were from LICOR. Blots were developed using LICOR Odyssey imager.

Mouse Models

Generation and characterization of iBIP mice and $RNF2^{L/L}$ mice are described in Supplementary Methods.

ChromHMM Analysis

We used ChromHMM (23) with default parameters to derive genome-wide chromatin state maps for all cell types, as described in our forthcoming study (Rai and colleagues, unpublished data). We binarized the input data with the ChromHMM's BinarizeBed method using a *P* value cutoff of $1e^{-4}$. We considered chromatin state models learned jointly on all chromatin marks at every increment of 5 states from 10 to 120 states. We chose a model with 45 states for

our main analysis to balance interpretability and capturing informative state distinctions for the analysis here. In particular, the model with 45 states was the model with the minimum number of states that was able to separate bivalent and poised states from active states.

Disclosure of Potential Conflicts of Interest

No potential conflicts of interest were disclosed.

Authors' Contributions

Conception and design: K. Rai, J.W. Horner, L. Chin
Development of methodology: K. Rai, J.W. Horner, A.J. Lazar
Acquisition of data (provided animals, acquired and managed patients, provided facilities, etc.): K. Rai, L.N. Kwong, E.Z. Keung, S. Sharma, N.S. Samant, J.B. Axelrad, A. Shah, D. Yang, A.J. Lazar
Analysis and interpretation of data (e.g., statistical analysis, biostatistics, computational analysis): K. Rai, K.C. Akdemir, P. Fiziev, C.-J. Wu, S. Sharma, D.R. Milton, J.W. Horner, A.J. Lazar, J. Ernst, L. Chin
Writing, review, and/or revision of the manuscript: K. Rai, K.C. Akdemir, L.N. Kwong, P. Fiziev, E.Z. Keung, E.A. Grimm, M.C. Barton, D.R. Milton, T.P. Heffernan, S. Ekmekcioglu, A.J. Lazar, J. Ernst, L. Chin
Administrative, technical, or material support (i.e., reporting or organizing data, constructing databases): S. Sharma, N.S. Samant, M. Williams, J.B. Axelrad, D. Yang, E.A. Grimm, J.W. Horner, S. Ekmekcioglu
Study supervision: J.W. Horner

Grant Support

The work described in this article was supported by grants from the NIH (5U01 CA141508 and U01 CA168394, to L. Chin; R01ES024995 and U01 HG007912, to J. Ernst), NCI (1K99CA160578-01, to K. Rai), Cancer Prevention and Research Institute of Texas (R1204, to L. Chin), and National Science Foundation (1254200, to J. Ernst). The following authors were supported by fellowships: K. Rai (Charles A. King postdoctoral fellowship), J. Ernst (Alfred P. Sloan fellowship), and P. Fiziev (California Institute for Regenerative Medicine Training Grant TG2-01169 and UCLA Training Program).

The costs of publication of this article were defrayed in part by the payment of page charges. This article must therefore be hereby marked *advertisement* in accordance with 18 U.S.C. Section 1734 solely to indicate this fact.

Received April 28, 2015; revised October 6, 2015; accepted October 6, 2015; published OnlineFirst October 8, 2015.

REFERENCES

1. Chi P, Allis CD, Wang GG. Covalent histone modifications–miswritten, misinterpreted and mis-erased in human cancers. Nat Rev Cancer 2010;10:457–69.
2. Leong SP, Gershenwald JE, Soong SJ, Schadendorf D, Tarhini AA, Agarwala S, et al. Cutaneous melanoma: a model to study cancer metastasis. J Surg Oncol 2011;103:538–49.
3. Scott KL, Nogueira C, Heffernan TP, van Doorn R, Dhakal S, Hanna JA, et al. Proinvasion metastasis drivers in early-stage melanoma are oncogenes. Cancer Cell 2011;20:92–103.
4. Tyler JK, Adams CR, Chen SR, Kobayashi R, Kamakaka RT, Kadonaga JT. The RCAF complex mediates chromatin assembly during DNA replication and repair. Nature 1999;402:555–60.
5. Thomas JO, Stott K. H1 and HMGB1: modulators of chromatin structure. Biochem Soc Trans 2012;40:341–6.
6. Vidal M. Role of polycomb proteins Ring1A and Ring1B in the epigenetic regulation of gene expression. Int J Dev Biol 2009;53:355–70.
7. Conaway RC, Conaway JW. The INO80 chromatin remodeling complex in transcription, replication and repair. Trends Biochem Sci 2009;34:71–7.
8. de Napoles M, Mermoud JE, Wakao R, Tang YA, Endoh M, Appanah R, et al. Polycomb group proteins Ring1A/B link ubiquitylation of histone H2A to heritable gene silencing and X inactivation. Dev Cell 2004;7:663–76.
9. Martinez-Romero C, Rooman I, Skoudy A, Guerra C, Molero X, Gonzalez A, et al. The epigenetic regulators Bmi1 and Ring1B are differentially regulated in pancreatitis and pancreatic ductal adenocarcinoma. J Pathol 2009;219:205–13.
10. Sanchez-Beato M, Sanchez E, Gonzalez-Carrero J, Morente M, Diez A, Sanchez-Verde L, et al. Variability in the expression of polycomb proteins in different normal and tumoral tissues. A pilot study using tissue microarrays. Mod Pathol 2006;19:684–94.
11. Garraway LA, Widlund HR, Rubin MA, Getz G, Berger AJ, Ramaswamy S, et al. Integrative genomic analyses identify MITF as a lineage survival oncogene amplified in malignant melanoma. Nature 2005;436:117–22.
12. Nguyen DX, Bos PD, Massague J. Metastasis: from dissemination to organ-specific colonization. Nat Rev Cancer 2009;9:274–84.
13. Talantov D, Mazumder A, Yu JX, Briggs T, Jiang Y, Backus J, et al. Novel genes associated with malignant melanoma but not benign melanocytic lesions. Clin Cancer Res 2005;11:7234–42.
14. McDonald OG, Wu H, Timp W, Doi A, Feinberg AP. Genome-scale epigenetic reprogramming during epithelial-to-mesenchymal transition. Nat Struct Mol Biol 2011;18:867–74.
15. Ben-Saadon R, Zaaroor D, Ziv T, Ciechanover A. The polycomb protein Ring1B generates self atypical mixed ubiquitin chains required for its in vitro histone H2A ligase activity. Mol Cell 2006;24:701–11.
16. Wang H, Wang L, Erdjument-Bromage H, Vidal M, Tempst P, Jones RS, et al. Role of histone H2A ubiquitination in Polycomb silencing. Nature 2004;431:873–8.
17. Kwong LN, Boland GM, Frederick DT, Helms TL, Akid AT, Miller JP, et al. Co-clinical assessment identifies patterns of BRAF inhibitor resistance in melanoma. J Clin Invest 2015;125:1459–70.
18. Meulmeester E, Ten Dijke P. The dynamic roles of TGF-beta in cancer. J Pathol 2011;223:205–18.
19. Bueno L, de Alwis DP, Pitou C, Yingling J, Lahn M, Glatt S, et al. Semi-mechanistic modelling of the tumour growth inhibitory effects of LY2157299, a new type I receptor TGF-beta kinase antagonist, in mice. Eur J Cancer 2008;44:142–50.
20. Todorovic V, Rifkin DB. LTBPs, more than just an escort service. J Cell Biochem 2012;113:410–8.
21. Hyytiainen M, Penttinen C, Keski-Oja J. Latent TGF-beta binding proteins: extracellular matrix association and roles in TGF-beta activation. Crit Rev Clin Lab Sci 2004;41:233–64.
22. Vehvilainen P, Hyytiainen M, Keski-Oja J. Latent transforming growth factor-beta-binding protein 2 is an adhesion protein for melanoma cells. J Biol Chem 2003;278:24705–13.
23. Ernst J, Kellis M. ChromHMM: automating chromatin-state discovery and characterization. Nat Methods 2012;9:215–6.
24. Bernstein BE, Mikkelsen TS, Xie X, Kamal M, Huebert DJ, Cuff J, et al. A bivalent chromatin structure marks key developmental genes in embryonic stem cells. Cell 2006;125:315–26.
25. Illingworth RS, Botting CH, Grimes GR, Bickmore WA, Eskeland R. PRC1 and PRC2 are not required for targeting of H2A.Z to developmental genes in embryonic stem cells. PloS One 2012;7:e34848.
26. Rao PS, Satelli A, Zhang S, Srivastava SK, Srivenugopal KS, Rao US. RNF2 is the target for phosphorylation by the p38 MAPK and ERK signaling pathways. Proteomics 2009;9:2776–87.
27. Eskeland R, Leeb M, Grimes GR, Kress C, Boyle S, Sproul D, et al. Ring1B compacts chromatin structure and represses gene expression independent of histone ubiquitination. Mol Cell 2010;38:452–64.
28. Qin Y, Ekmekcioglu S, Liu P, Duncan LM, Lizee G, Poindexter N, et al. Constitutive aberrant endogenous interleukin-1 facilitates inflammation and growth in human melanoma. Mol Cancer Res 2011;9:1537–50.
29. Garber M, Yosef N, Goren A, Raychowdhury R, Thielke A, Guttman M, et al. A high-throughput chromatin immunoprecipitation approach reveals principles of dynamic gene regulation in mammals. Mol Cell 2012;47:810–22.